Journal of Geoscience and Environment Protection, 2024, 12, 73-101
https://www.scirp.org/journal/gep
ISSN Online: 2327-4344
ISSN Print: 2327-4336

Hydrochemical Assessment of Groundwater and Dominant Water-Rock Interactions in Ooeides Aquifer System, North Greece

Adam Adamidis[1], Ioannis Gkiougkis[1*], Andreas Kallioras[2], Panagiotis Angelidis[1], Fotios-Konstantinos Pliakas[1]

[1]Laboratory of Engineering Geology and Groundwater Research, Department of Civil Engineering, Democritus University of Thrace, Xanthi, Greece
[2]School of Mining and Metallurgical Engineering, National Technical University of Athens, Athens, Greece
Email: *jgiougis@civil.duth.gr

How to cite this paper: Adamidis, A., Gkiougkis, I., Kallioras, A., Angelidis, P., & Pliakas, F.-K. (2024). Hydrochemical Assessment of Groundwater and Dominant Water-Rock Interactions in Ooeides Aquifer System, North Greece. *Journal of Geoscience and Environment Protection, 12,* 73-101.
https://doi.org/10.4236/gep.2024.1211005

Received: September 30, 2024
Accepted: November 17, 2024
Published: November 20, 2024

Abstract

This paper deals with the assessment of main controls on groundwater chemistry in the aquifer system of Ooeides, Orestiada Region, NE Greece, contributing to the assessment of groundwater and surface water interaction, as well as water-rock interactions in the study area. Statistical analysis and relevant hydrochemical plots were employed in the analysis of groundwater samples from the study area during sampling campaigns for the years 2018, 2019 and 2020. The process included the collection and analysis of hydrochemical, hydrological and hydrogeological information and data regarding the aquifer system of the study area. Based on the statistical processing and the spatial analysis of the relevant results of the research, interesting and useful information emerged regarding: i) the recharge procedure of the aquifer from surface water of rivers and streams in the study area; ii) the relationship of groundwater composition with the type of rock through which water flows; iii) the impact on groundwater quality from anthropogenic activities (cultivation activities, municipal waste). From the elaboration of all the above, interesting findings and suggestions came out, which are considered useful for the optimal management of the hydrogeological regime of the study area.

Keywords

Groundwater Hydrochemical Analysis, Conjunctive Use of Surface Water and Groundwater, Water-Rock Interaction, Orestiada, Greece

1. Introduction

According to Razi et al. (2024), groundwater's geochemical content is influenced

by human actions at the surface, climate factors, and the quality of replenishment water. In addition, Dong and Gao (2022) report that human activities, industrial development, increased water demand due to population growth, and groundwater overexploitation alter the environment around groundwater, resulting in changes in the chemical components of groundwater. Liu et al. (2022) mention that natural causes play an important influence in the evolution of groundwater chemistry. Also, while manmade disturbances may have a significant impact on groundwater chemistry during comparatively short times, the natural exchange of atmospheric water, surface water, and groundwater typically takes place over a lengthy geological period.

Razi et al. (2024) state that hydrogeochemical research has shown that a variety of geogenic factors can alter the chemical composition and general quality of groundwater as it moves from recharge to discharge zones (Dong & Gao, 2022; Liu et al., 2022). Because groundwater naturally interacts with rocks and soils, different minerals can be found in dissolved ions as well as non-ionic solutions (Ansari et al., 2019). Thus, processes involving the interaction of water and rock, such as ion exchange, weathering, evaporation, and mineral dissolution, also influence the geochemistry of groundwater (Tesfamichael, 2011; Liu et al., 2022; Sunkari et al., 2022; Ribinu et al., 2023).

The groundwater's elemental concentration fluctuations are largely caused by geochemical processes such as adsorption, cation exchange, and the dissolution and precipitation of solids. Therefore, the concentrations of major ions in groundwater can be used to determine the strength and type of water-rock interactions and chemical reactions (Elango & Kannan, 2007).

Furthermore, Belkhiri et al. (2012) point out that hydrochemical processes provide a better understanding of the contribution of rock-water interactions and human influences on groundwater quality.

Groundwater resources play the most important role in the supply of irrigation water to rural communities in Orestiada Region in Evros Prefecture, NE Greece, while surface water sources are related to rivers Evros and Ardas. The groundwater hydrochemical status of the hydrogeological system of Orestiada region is investigated using updated data in addition to information and data from previous relevant research in the wider study area (Diamantis & Pliakas, 2013; Government Gazette-GG 4680/B'/29.12.2017; Papadopoulos & Romaidis, 2022; Adamidis et al., 2023). This research work deals with the assessment of groundwater quality and main controls on groundwater chemistry in the aquifer system of Ooeides, Orestiada Region contributing to the assessment of groundwater and surface water interaction, as well as water-rock interactions in the study area focusing mainly on groundwater, which is considered the most influencing assessment factor. Statistical analysis and relevant hydrochemical plots were employed in the analysis of groundwater samples from the study area during sampling campaigns for the years 2018, 2019 and 2020. From the elaboration of all the above, interesting findings and suggestions came out, which are considered useful for the optimal

management of the hydrogeological regime of the study area.

2. Study Area, Geological and Hydrological Information

The study area is located in River Evros Trough, Orestiada Region in Evros Prefecture, NE Greece (**Figure 1**) covering a narrow land strip of 160 km^2, called "Ooeides", which in Greek means oval because of its shape, with variation of altitude values from south to north: 22 m - 35 m. The eastern border is River Evros. Irrigation needs for rural activities are met by pumping of groundwater from over a hundred wells, then supplied through a pipe network. Three hundred and fifty (350) wells are located within the area with discharge flow values varying from 50 to150 m^3/h. The population of the settlements located at the western border of the study area amounts to 22994 people (census 2021), where water supply is covered by a network of wells outside the study area. The water of the study area is used exclusively for irrigation. The estimated quantities of water pumped in the years 2018, 2019 2020 are 1.54×10^6 m^3, 1.71×10^6 m^3, 1.99×10^6 m^3, respectively.

The lithological composition of the study area is made up of Holocene alluvials, consisting of alternations of cobbles, sands, gravels and clays in interlocking horizons in vertical and horizontal sense creating a heterogeneity in the material (**Figure 1**) (Andronopoulos, 1977; Tsirambides et al., 1993; Koutles et al., 1995; Adamidis et al., 2022a). According to Adamidis et al. (2022b), the sedimentation of Plio-Plistocene represents the main formation of the study area. Located to the edges of River Ardas basin and the Neochori stream basin, continues submerged under the alluvial depositions.

Three stream basins drain into the western part of the study area; the northern one on the area of 69.10 km^2 with a lithological basement mainly of conglomerates, and the southern one on the area of 72.07 km^2, which is developed on a basement of conglomerates and sandstone. The central one is the basin of the Neochorio stream with an area of 119,559 km^2, which develops on alluvial basement. The values of the HORTON index, which index describes physical parameters of a drainage basin are less than 0.5 (0.07 for the northern, 0.09 for the Neochorio stream basin and 0.1 for the southern basin), so they are characterized as very elongated. In addition, due to the elongated shape, the water flow time within the basin increases and, in combination with the lithology of the basement, infiltration is favored. The alluvial deposits are included in the hydrological basin of the River Evros.

Within the alluvial formations, with sharp vertical and lateral transitions of the grain size of the materials, and alternations of fine-grained and steep materials, unconfined and leaky confined aquifers develop (**Figure 2**, **Figure 3**). The presence of fine-grained impervious layers at various stratigraphic heights, although it may locally create a blockage of the flow in terms of its vertical component, does not cause a complete interruption of the hydraulic communication between the aquifers. The recharge of the alluvial formations is mainly ensured by the infiltration of river water, by the infiltration of the Plio-Pleistocene formation and

Pleistocene formations of sandstones and to a very small extent by the infiltration of precipitation (Diamantis & Pliakas, 2013).

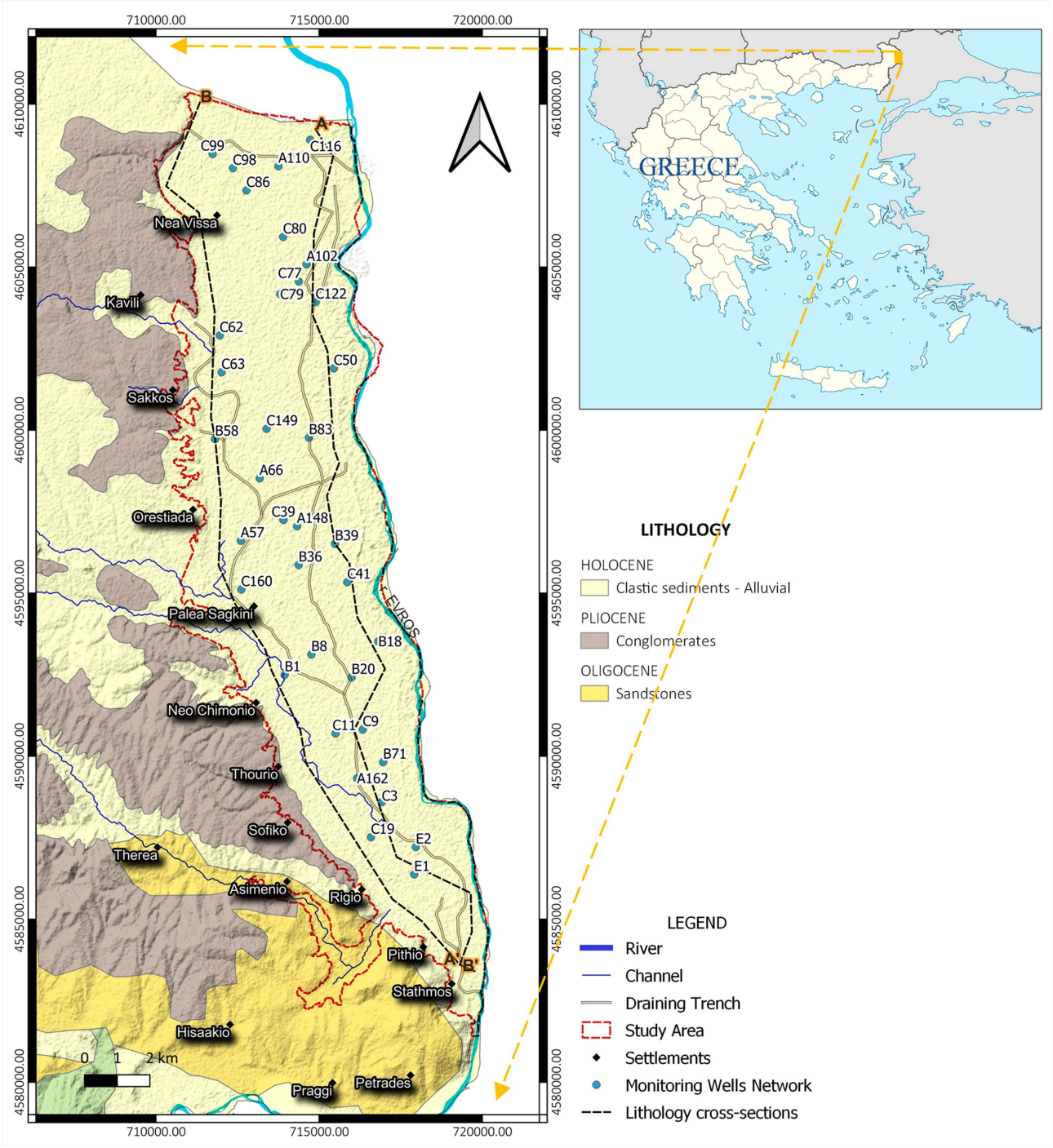

Figure 1. Study area, geological map of the study area (dashed red line), monitoring wells and settlements and cross sections axes A-A' (**Figure 2**), B-B' (**Figure 3**) (Greece map: https://en.m.wikipedia.org/wiki/File:Greece_location_map.svg).

3. Materials and Methods

The intention of this research work is to focus on the evaluation of surface water

and groundwater interactions, as well as water-rock interactions in the studied aquifer system coming up with results including data, information, findings, valuations and proposals, which are considered very useful for the development and management of groundwater and surface waters at the study area. The research hopes to contribute to the possible efforts for the conjunctive use and management of groundwater and surface water in the wider area.

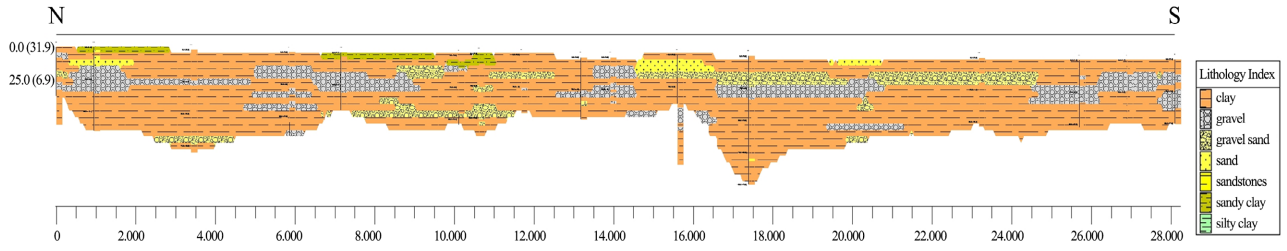

Figure 2. Cross section north to south at the eastern boundary of the study area (A-A' axis in **Figure 1**).

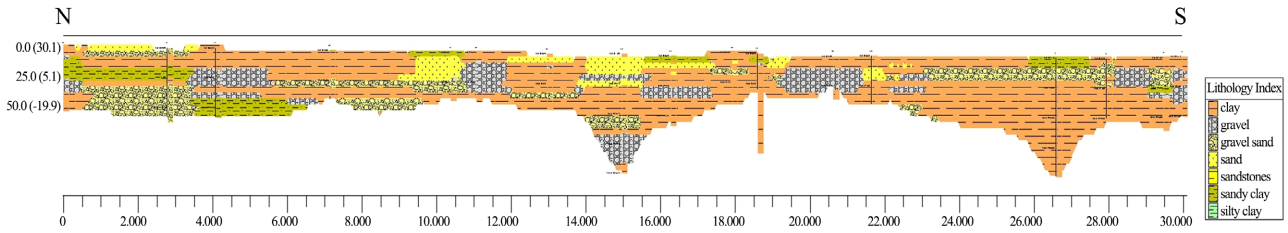

Figure 3. Cross section north to south at the western boundary of the study area (B-B' axis in **Figure 1**).

3.1. Meteorological Data

The evolution of groundwater potential is inextricably linked to the surface hydrology and mainly to the long-term course of rainfall. The hydrological conditions of an area depend on two main factors, its climate and its geological structure.

The meteorological data that were used in this paper concern the Meteorological Station of Orestiada which is included in the network of stations of the National Observatory of Athens, for the time period 10/2006 to 12/2020 (http://stratus.meteo.noa.gr). Additional data were obtained from the POWER|DAVe (NASA) digital database for the period January 1981 to December 2020 (https://power.larc.nasa.gov/beta/data-access-viewer/).

The meteorological data concern the values of average monthly precipitation, average monthly temperature, maximum monthly temperature, minimum monthly temperature. The data were processed with the software Hydrognomon 4. **Figure 4** shows the locations of the meteorological station of Orestiada and the locations of the points for which data were received from POWER|DAVe (NASA). The latter are based on satellites and models and have proven to be accurate enough to provide reliable solar and meteorological data in areas where surface measurements are sparse or non-existent, such as in the study area.

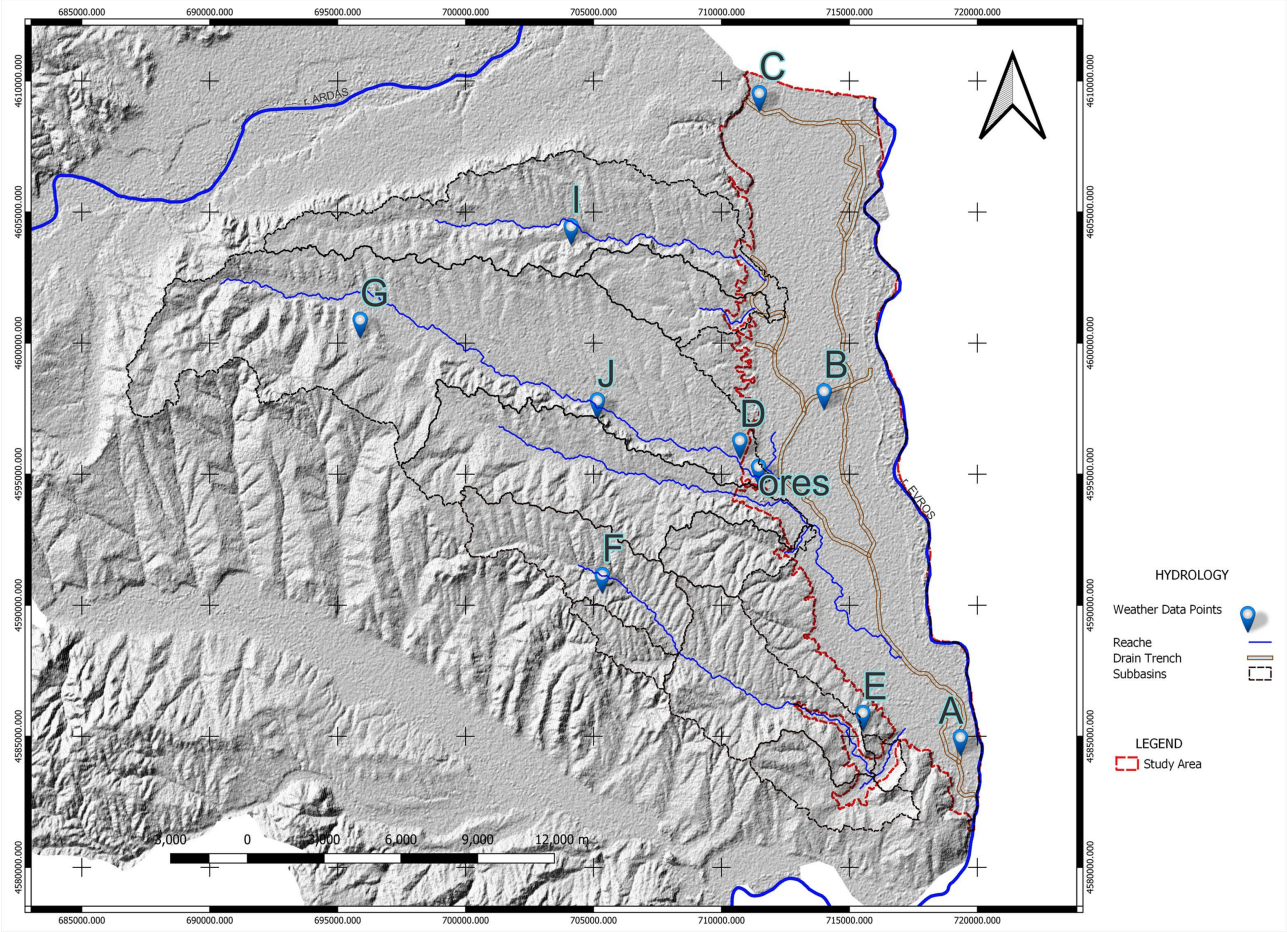

Figure 4. Locations of meteorological stations.

The data from the base POWER|DAVe (NASA) offer two unique features: they are global and generally continuous in time. For the study area they provide continuous data for the period 1981-2020.

3.2. Groundwater Level Measurements and Groundwater Sampling

In May/June and November/December, of each of three years 2018, 2019, 2020, groundwater level measurements were performed at thirty-six (36) wells. Additionally, in August, groundwater sampling from thirty (30) wells in the study area was performed, followed by chemical analyses. The relevant research included: i) groundwater level measurements and piezometric maps design (May and December) based on the relevant measurement data collected from the aforementioned monitoring network of thirty-six (36) wells, ii) groundwater sampling and chemical analysis, and design of relevant hydrochemical diagrams and maps.

Piezometric maps of the aquifer of the study area, which is characterized as leaky aquifer and, in places, unconfined aquifer, were designed using Simple Kriging geostatistical interpolation method (May and November 2018, May and December 2019, June and November 2020) (Figure 5, Figure 6).

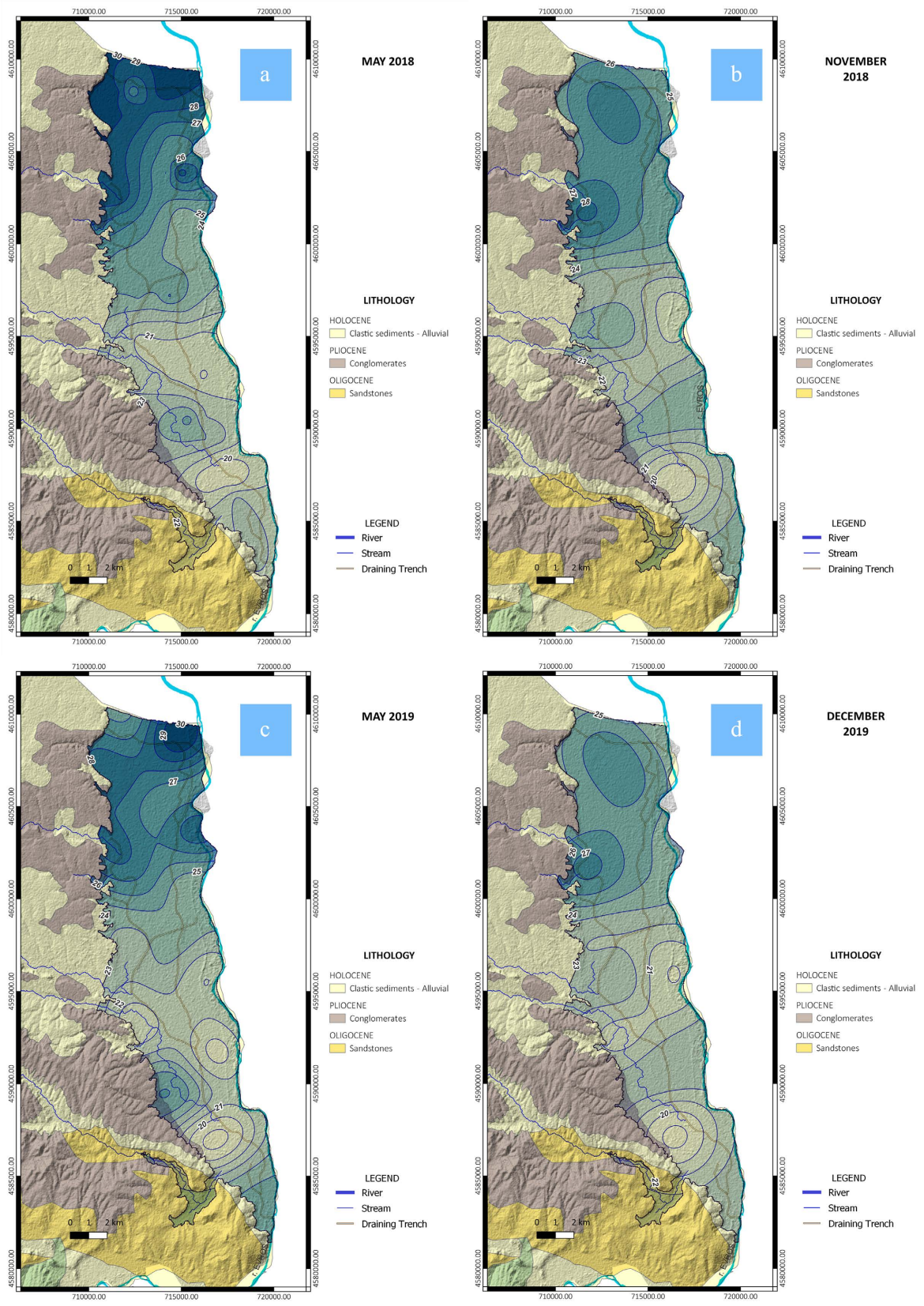

Figure 5. Piezometric maps of the aquifer of the study area (groundwater level in m (a.s.l.) (a: May 2018; b: November 2018; c: May 2019; d: December 2019).

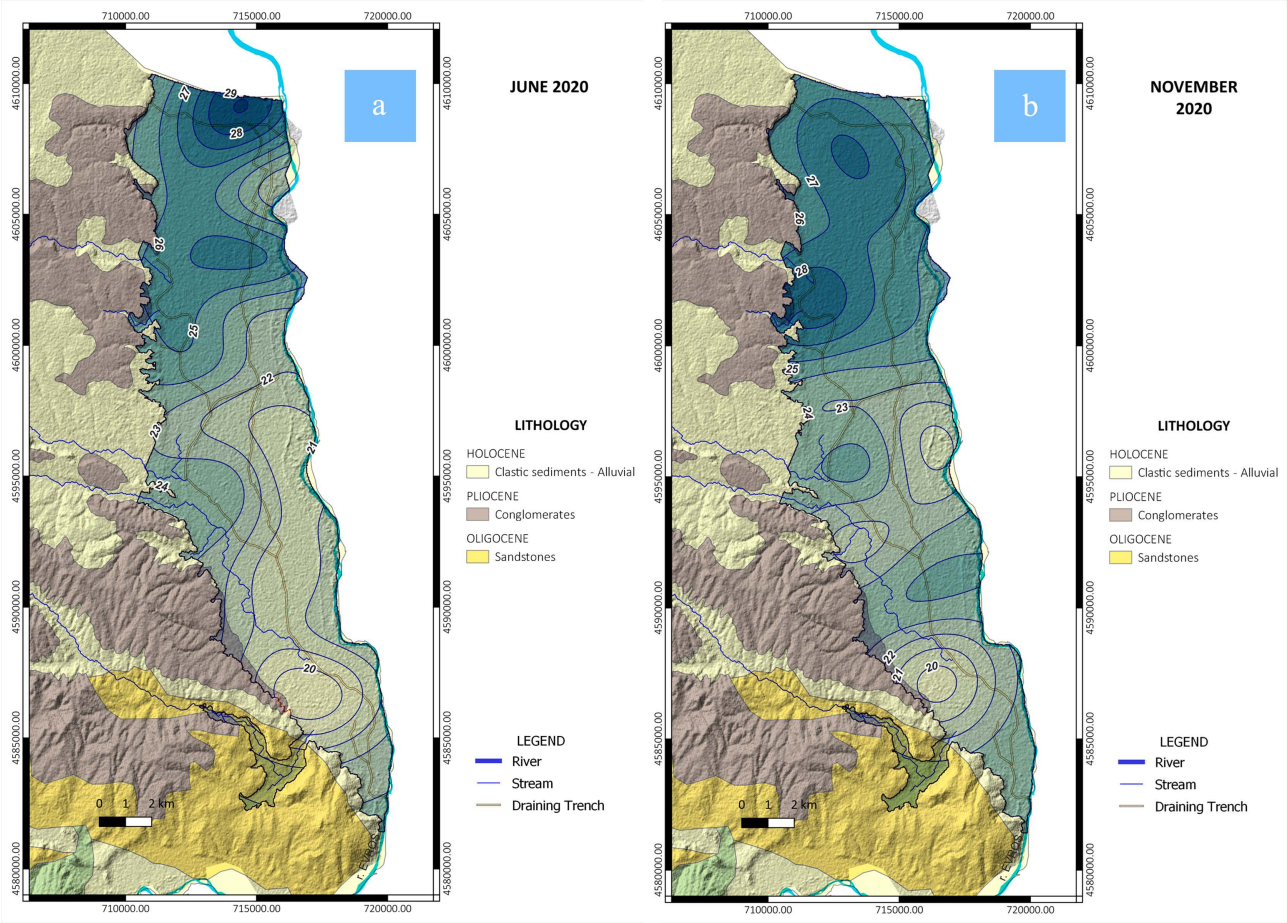

Figure 6. Piezometric maps of the aquifer of the study area (groundwater level in m (a.s.l.) (a: June 2020; b: November 2020).

In the context of the development of the conceptual model of the study area, hydrochemical research was carried out in a network of thirty (30) monitoring wells. Three groundwater sampling campaigns were performed in August of 2018, 2019 and 2020. The relevant groundwater chemical analyses were carried out at the Laboratory of Engineering Geology and Groundwater Research, Department of Civil Engineering, DUTH. The chemical parameters examined were the following: Ca^{2+}, Mg^{2+}, SO_4^{2-}, HCO_3^-, PO_4^{3-}, NO_3^-, NO_2^-, NH_4^+, Cl^-, Electrical Conductivity (EC), Total Dissolved Solids (TDS), pH, K^+, Na^+, Fe^{2+}, Mn^{2+}.

4. Results and Discussion

Figure 7 shows the spatial distribution of the mean annual precipitation in the study area, as well as in the watersheds of the streams flowing into the study area.

Figure 8 shows the variation of the mean monthly precipitation, the relevant cumulative curve of precipitation and the mean monthly temperature values for the period 1981-2020. The maximum mean monthly precipitation value was recorded in January 1995 with a value of 157 mm. The year with the highest mean value of spatial precipitation is 2014 with a value of 777.14 mm. The mean annual

spatial precipitation of 2018 is reduced by 1.14 mm compared to 2017. In 2019 it is reduced by 262.47 mm from 2018, while in 2020 it is increased by 22.41 mm from 2019 and in 2020 (456.71 mm) the mean spatial rainfall values are smaller than the value of 504.14 mm, which is the mean extended spatial height of precipitation in the study area. In the period 2019-2020, the annual amount of precipitation corresponds to 62% - 68% of the annual precipitation in 2018.

Figure 9 presents the mean monthly temperature in the period 1981-2020. Spatial mean monthly temperature values range between 2.48˚C in January to 26.94˚C in July. In the period 1981-2020, the average maximum spatial temperature is noted in July 2012 with a value of 30.73˚C, with a minimum value of −3.00˚C in December 2011. The year with the highest mean temperature value is 2019 with a value of 15.91˚C and the year with the lowest mean annual temperature value is the year 1982 with 13.00˚C. The mean annual temperature changes in the period under study are an increase by 0.53˚C from 2017 to 2018, an increase by 0.56˚C from 2018 to 2019 and a decrease by 0.18˚C from 2019 to 2020. The mean annual temperature values in 2018 (15.35˚C), 2019 (15.91˚C) and 2020 (15.73˚C) are higher than the mean annual spatial temperature in the study area with a value of 14.24˚C.

From the analysis of the piezometric maps (Figure 5, Figure 6), it appears that the groundwater system is recharged constantly from the middle west part of the area. Groundwater flow direction is detected towards the Evros River and the alluvial deposits at the northern and southeastern boundary of the area, mainly. At the western boundary, the aquifer system is recharged by surface water from streams whose catchments are located within the conglomerates and sandstones.

The statistical processing of the of chemical analysis results for the three time periods 2018, 2019, 2020 is presented in Table 1, which contains the minimum, maximum values, standard deviation and mean values of the main ions.

In Table 1, values of standard deviation greater than the mean value in the concentrations of Fe^{2+}, NO_3^- and NO_2^- ions are noted (in bold), expressing the origin of the ions from different sources apart from natural processes possibly from anthropogenic activities.

In concentration data where standard deviation values greater than the mean are noted, as well as in concentrations of ions with possible anthropogenic causes, an independent samples T-test was performed with a null hypothesis that the mean concentration values are equal (Table 2). Rejecting the null hypothesis expresses that the cause of the concentration value of the ion is some other cause than physical processes. The control was carried out for the concentrations of K^+, Mn^{2+}, NH_4^+, Cl^-, NO_3^-, NO_2^-, PO_4^{3-} ions with a 95% confidence interval value.

The null hypothesis is rejected for the Fe^{2+}, NH_4^+ and PO_4^{3-} samples of the 2018-2019 periods, while for the 2019-2020 period, the null hypothesis is rejected for the concentrations of Fe^{2+} ions. It can therefore be considered that the causes

of Fe^{2+}, NH_4^+ and PO_4^{3-} concentration values are also other than the natural processes within the aquifer in the period 2018-2019, as well as for the period 2019-2020 for Fe^{2+}.

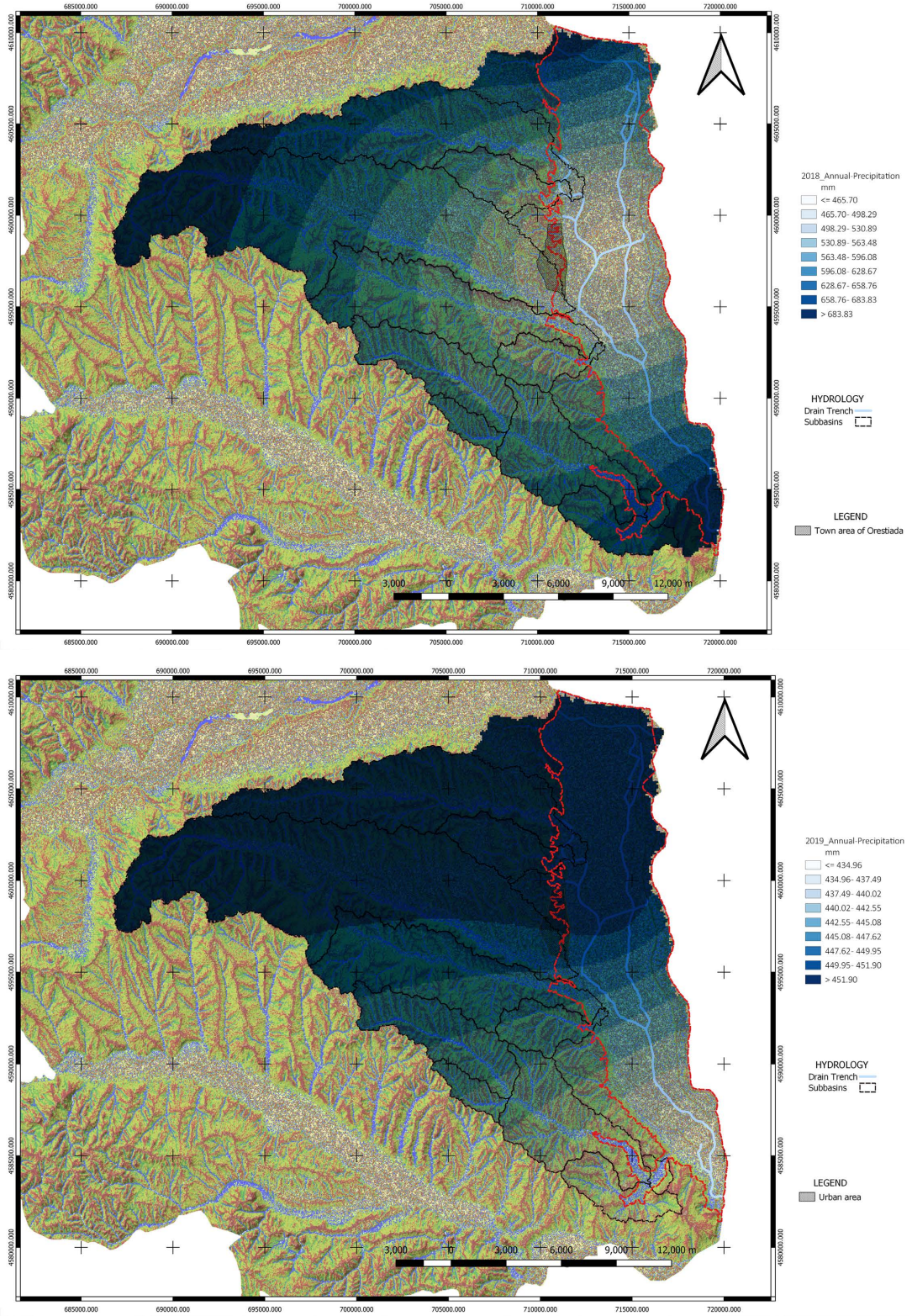

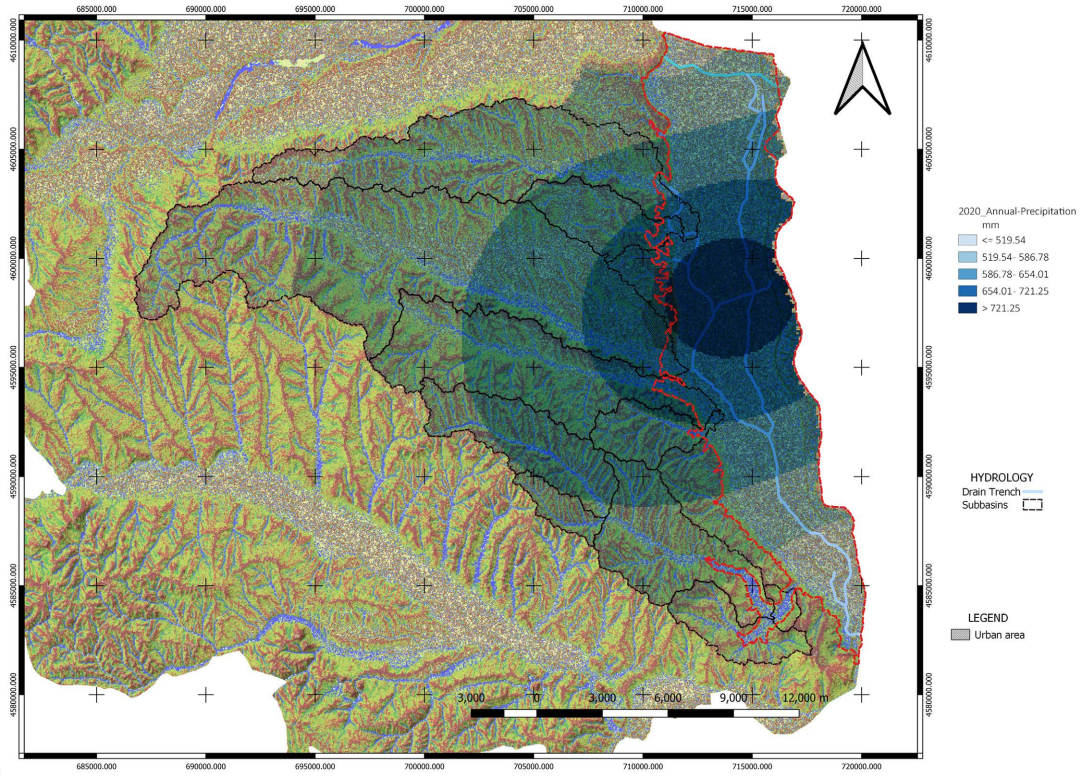

Figure 7. Annual precipitation values distribution (upper: 2018, middle: 2019, lower: 2020).

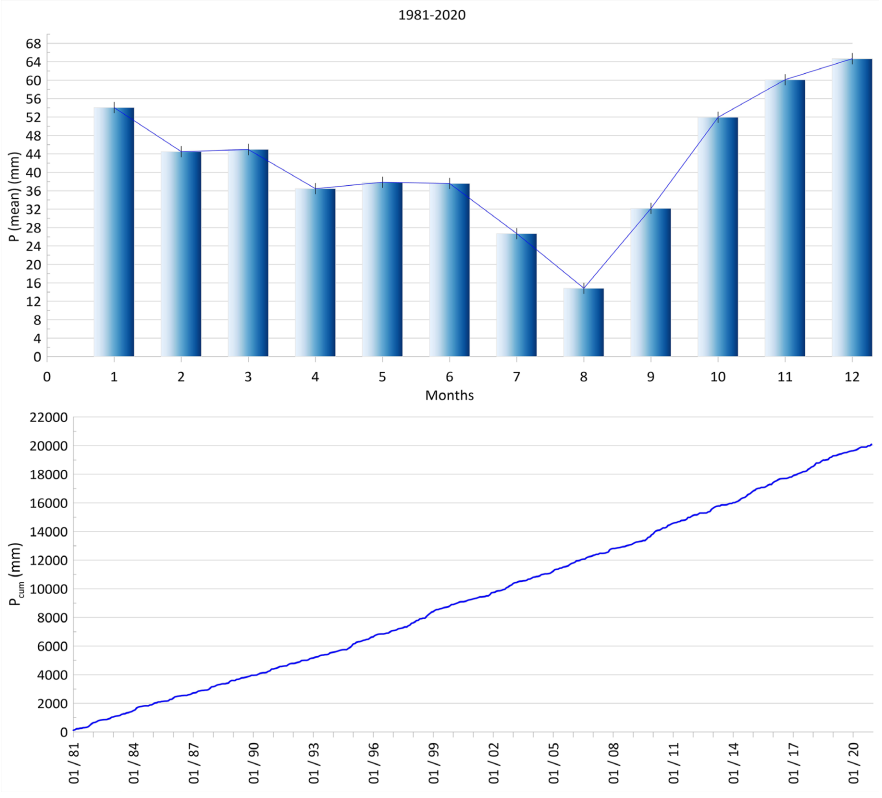

Figure 8. Mean monthly precipitation (upper) and cumulative curve of precipitation (lower) for the period 1981-2020.

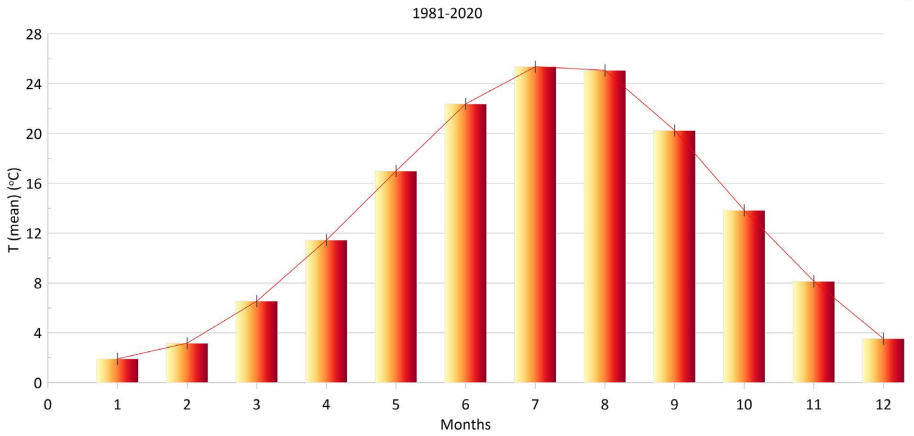

Figure 9. Mean monthly temperature (oC) for the period 1981-2020.

The correlation results of the hydrochemical parameters are presented in **Table 3**. All hydrochemical parameters were standardized to z-scale as shown in Equation (1) below (Aruga et al., 1995; Avtar et al., 2011; Singh et al., 2018). This is a preliminary step to avoid variation range differences. Hydrochemical data are normally distributed (Liu et al., 2003; Singh et al., 2004; Ledesma-Ruiz et al., 2015). The relationship between hydrochemical parameters was examined by creating a correlation matrix accepting significance at the $P < 0.01$ level.

$$z_i = \frac{x_i - \overline{x}}{stdv_i} \tag{1}$$

where, z_i is a standardized variable, x_i is the raw variable, $\overline{x}$ is the mean value, and $stdv_i$ is the standard deviation.

In the correlation matrix, Ca^{2+} shows a strong positive correlation with HCO_3^- (0.89), Cl^- (0.73) and Mg^{2+} (0.74) in 2018. This relationship may indicate the dissolution of minerals (anhydrite, anorthosite) which are a source of Ca^{2+} (Malenda, 2019). These correlations are not present in 2019, while in 2020 the correlation reappears with HCO_3^- (0.91) and with Mg^{2+} (0.77). This relationship may indicate the dissolution of minerals (gypsum) which are a source of Ca^{2+}. Mg^{2+} shows in all periods a stable positive correlation with HCO_3^-. In the 2019 samples, it shows a positive correlation with SO_4^{2-} (0.78) and in the 2020 samples with NH_4^+ (0.70). The correlation with SO_4^{2-}, suggests that these ions originate from anthropogenic contamination (Mu et al., 2015), such as sewage and sulfur deposition from industrial processes (Zhang et al., 2016), as well as from geological factors, such as the occurrence/effect of sodium sulfate-bearing minerals in sedimentary minerals (Salyapongse et al., 2022), as well as the presence of marls and gypsum. In 2018, samples Cl^- show a strong positive correlation with NO_3^- (0.75) while in the 2019 samples Fe^{2+} showed a strong positive correlation with Mn^{2+}. implying that groundwater may be contaminated by sewage and fertilizers (Hem, 1985; Choi, 1988).

The TDS values range in minimum values from 126 mg/L, with maximum values from 1197 to 1218 mg/L while the mean value ranges from 492 to 732 mg/L.

In the second sampling campaign there is an increase in TDS values compared to the first and third sampling. This may be due to the reduction of groundwater recharge from precipitation and surface water because in 2019, a decrease in the amount of precipitation and an increase in temperature were observed, so the TDS values may be affected by water-rock interaction. TDS values > 1000 mg/L which is a limit for fresh water is noted at a rate of 3% in the first period, 14% in the second and 7% on the third period. The pH values range from 6.61 to 8.36 with an average value of 7.37, indicating slightly acidic conditions. In the first period, the lowest values are noted and therefore the most acidic conditions.

Table 1. Statistical processing of chemical analysis results (August 2018, 2019, 2020).

	2018				2019				2020			
	Mean	StdDv	Min	Max	Mean	StdDv	Min	Max	Mean	StdDv	Min	Max
pH	7.25	0.33	6.61	7.90	7.45	0.18	7.06	7.71	7.43	0.31	6.71	8.36
EC	757.97	381.90	195.00	1843.00	891.14	253.26	401.00	1285.00	772.63	259.03	378.00	1258.00
TDS	492.68	248.24	126.75	1197.95	732.77	233.02	268.45	1218.11	659.11	253.97	282.90	1205.19
Ca^{2+}	93.13	54.10	17.64	250.10	52.00	15.03	19.64	78.56	87.35	43.58	17.64	173.15
Mg^{2+}	24.23	14.19	3.89	68.04	45.81	20.94	7.05	99.63	29.00	12.51	9.72	58.32
Na^{+}	5.08	1.68	2.72	8.39	64.84	31.06	31.30	198.00	60.37	13.76	27.00	84.80
K^{+}	3.02	1.60	1.00	8.10	4.43	5.22	1.00	30.00	2.79	1.11	1.23	5.50
Mn^{2+}	1.34	1.41	0.20	6.50	2.16	1.91	bdl	6.80	1.80	1.31	bdl	4.90
Fe^{2+}	0.17	0.19	bdl	0.69	0.84	1.00	bdl	3.28	0.27	1.03	bdl	5.40
NH_4^+	0.30	0.42	bdl	1.98	0.63	0.63	0.02	1.95	0.50	0.29	0.13	1.54
HCO_3^-	345.24	177.08	71.98	722.24	407.86	131.35	137.25	613.66	351.80	147.24	131.76	677.10
Cl^-	55.33	34.34	19.50	177.30	52.62	30.72	23.05	161.34	40.35	23.54	13.50	117.02
SO_4^{2-}	73.84	31.60	5.00	112.60	97.88	54.39	11.20	195.00	74.91	51.90	7.00	204.00
NO_3^-	4.17	9.69	bdl	46.00	2.68	5.58	bdl	22.00	9.08	25.18	bdl	130.00
NO_2^-	0.21	0.40	bdl	1.76	0.10	0.28	bdl	1.24	0.02	0.02	bdl	0.06
PO_4^{3-}	0.29	0.18	0.08	0.78	0.94	0.74	0.25	3.00	0.89	0.44	0.36	1.80

bdl: below detection limit.

Table 2. Independent Sample T-test.

Ions	2018-2019			2019-2020		
	Lower	Upper	Control	Lower	Upper	Control
K^{+}	−3.44	0.63	Ho = 0	−0.42	3.70	Ho = 0
Mn^{2+}	−1.71	0.07	Ho = 0	−0.53	1.25	Ho = 0
Fe^{2+}	−1.05	−0.29	Ho ≠ 0	0.02	1.12	Ho ≠ 0
NH_4^+	−0.62	−0.05	Ho ≠ 0	−0.14	0.40	Ho = 0
Cl^-	−14.61	20.03	Ho = 0	−2.58	27.10	Ho = 0
NO_3^-	−2.72	5.71	Ho = 0	−16.18	3.38	Ho = 0
NO_2^-	−0.08	0.29	Ho = 0	−0.02	0.19	Ho = 0
PO_4^{3-}	−0.93	−0.36	Ho ≠ 0	−0.28	0.39	Ho = 0

As shown in Table 1, the concentration of cations in the samples of the first sampling follows the order $Ca^{2+} > Mg^{2+} > Na^{+} > K^{+}$. In the 2019, 2020 sampling results the order $Na^{+} > Mg^{2+} > Ca^{2+} > K^{+}$, $Ca^{2+} > Na^{+} > Mg^{2+} > K^{+}$, $Mg^{2+} > Ca^{2+} > Na^{+} > K^{+}$, and $Mg^{2+} > Na^{+} > Ca^{2+} > K^{+}$ is followed. The order $HCO_3^- > SO_4^{2-} > Cl^-$, $HCO_3^- > Cl^- > SO_4^{2-}$ regarding concentration of the anions is followed in all sampling periods. The predominance of HCO_3^- strengthens the finding that the aquifer system is recharged by surface water of River Evros and streams. Changes in the order of cations and anions imply the different types of water within the study area and may indicate the difference in certain geochemical processes (such as evaporation or water-rock interactions) occurring in different water types.

Table 3. Correlation Matrix (2018, 2019, 2020).

2018	Ca^{2+}	Mg^{2+}	Na^{+}	K^{+}	Mn^{2+}	Fe^{2+}	NH_4^+	HCO_3^-	Cl^-	SO_4^{2-}	NO_3^-	NO_2^-	PO_4^{3-}
Ca^{2+}	1.00												
Mg^{2+}	0.74	1.00											
Na^{+}	0.12	0.16	1.00										
K^{+}	0.44	0.33	−0.10	1.00									
Mn^{2+}	0.42	0.42	0.52	0.13	1.00								
Fe^{2+}	0.11	−0.10	0.15	−0.03	0.04	1.00							
NH_4^+	0.43	0.31	0.42	0.14	0.86	0.11	1.00						
HCO_3^-	0.89	0.75	0.36	0.28	0.61	0.10	0.56	1.00					
Cl^-	0.73	0.68	−0.16	0.52	0.04	0.18	0.01	0.43	1.00				
SO_4^{2-}	0.56	0.57	0.01	0.36	0.30	−0.10	0.33	0.38	0.48	1.00			
NO_3^-	0.51	0.50	−0.39	0.35	−0.17	−0.16	−0.13	0.18	0.75	0.39	1.00		
NO_2^-	0.18	0.15	0.34	0.02	0.44	0.40	0.37	0.32	0.03	0.02	−0.14	1.00	
PO_4^{3-}	0.05	−0.03	0.16	0.14	0.04	−0.16	0.15	0.21	−0.26	−0.24	−0.09	0.00	1.00
2019	Ca^{2+}	Mg^{2+}	Na^{+}	K^{+}	Mn^{2+}	Fe^{2+}	NH_4^+	HCO_3^-	Cl^-	SO_4^{2-}	NO_3^-	NO_2^-	PO_4^{3-}
Ca^{2+}	1.00												
Mg^{2+}	0.41	1.00											
Na^{+}	0.19	0.34	1.00										
K^{+}	0.03	0.13	0.85	1.00									
Mn^{2+}	0.10	0.58	0.25	−0.01	1.00								
Fe^{2+}	0.04	0.33	0.23	0.05	0.80	1.00							
NH_4^+	−0.03	0.27	0.44	0.38	0.65	0.55	1.00						
HCO_3^-	0.58	0.71	0.57	0.33	0.60	0.43	0.56	1.00					
Cl^-	0.18	0.32	0.73	0.69	−0.15	−0.13	0.12	0.35	1.00				
SO_4^{2-}	0.52	0.78	0.35	0.15	0.56	0.53	0.16	0.63	0.25	1.00			
NO_3^-	−0.09	−0.04	−0.18	−0.06	−0.38	−0.39	−0.40	−0.44	0.17	−0.02	1.00		
NO_2^-	0.01	0.09	−0.04	−0.04	0.10	−0.09	0.22	0.26	0.03	−0.05	−0.16	1.00	
PO_4^{3-}	0.00	0.43	0.62	0.60	0.52	0.58	0.68	0.56	0.37	0.36	−0.27	−0.13	1.00

Continued

2020	Ca^{2+}	Mg^{2+}	Na^{+}	K^{+}	Mn^{2+}	Fe^{2+}	NH_4^{+}	HCO_3^{-}	Cl^{-}	SO_4^{2-}	NO_3^{-}	NO_2^{-}	PO_4^{3-}
Ca^{2+}	1.00												
Mg^{2+}	0.77	1.00											
Na^{+}	0.45	0.41	1.00										
K^{+}	0.51	0.34	0.45	1.00									
Mn^{2+}	0.41	0.35	0.28	−0.09	1.00								
Fe^{2+}	0.03	0.02	−0.03	−0.18	0.48	1.00							
NH_4^{+}	0.64	0.70	0.24	0.34	0.40	0.23	1.00						
HCO_3^{-}	0.91	0.74	0.49	0.41	0.37	0.04	0.68	1.00					
Cl^{-}	0.07	0.33	0.43	0.05	0.17	−0.14	−0.05	−0.02	1.00				
SO_4^{2-}	0.77	0.69	0.34	0.60	0.15	0.04	0.66	0.61	0.09	1.00			
NO_3^{-}	0.26	0.10	0.25	0.14	0.44	−0.06	0.25	0.24	0.08	0.19	1.00		
NO_2^{-}	0.13	0.00	−0.21	0.04	0.26	0.15	0.05	0.03	−0.36	0.03	−0.03	1.00	
PO_4^{3-}	−0.15	−0.02	−0.34	−0.09	0.03	0.42	0.01	−0.19	0.02	−0.01	0.00	0.35	1.00

The quality of groundwater is determined mainly by the lithology of the geological formations through which it flows. Consequently, aquifers in different rocks represent waters of different hydrochemical types. **Figure 10** shows the spatial distribution of the hydrochemical types of groundwater based on the results of chemical analyzes for each sampling period, while **Figure 11** presents spatial distribution of TDS values for each campaign. It is pointed out that Simple Kriging is the geostatistical interpolation method used to design all hydrochemical maps.

Most of the 2018 groundwater samples at a rate of 92% are dominated by Ca–HCO_3, indicating the dominance of alkaline earth metals over alkalis (Ca^{2+} > Mg^{2+} > Na^{+} > K^{+}), while 3% are of type fresh water Ca-Cl and 7% Ca-SO_4. The samples in 2019 are of Ca-HCO_3 type at a rate of 15%, of Mg-HCO_3 fresh groundwater type at a rate of 71% and of Na-HCO_3 type at a rate of 14%, while the samples in 2020 are of Ca-HCO_3 type at a rate of 74%, of Mg-HCO_3 freshwater type at a rate of 7% and of Na-HCO_3 type at a rate of 19%. Groundwater of Na-HCO_3 type with correspondingly high TDS values (1041.8 mg/L), confirm this groundwater type had more time to interact with the rock matrix and the surrounding environment and are located at the contact of the alluvium with the sandstones in the southwestern part of the study area in the 2019 period. In an ordinary hydrochemical mechanism, groundwater from limestone belongs to the Ca-HCO_3 hydrochemical type, while from dolomite to the Mg-HCO_3 type. In cases where the carbonate rocks contain gypsum layers, the dominant type of water is Ca-Mg-HCO_3-SO_4. The cations Ca^{2+}, Mg^{2+}, Na^{+} represent 74% of ions of 2018, 22% of 2019 and 27% of 2020. The anions HCO_3^{-}, Cl^{-}, SO_4^{2-} represent 26% of ions of 2018, 76% of 2019 and 71% of 2020. It is remarkable that the 71% of cations of 2018 represented by Ca^{2+}, 7% and 13% of 2019, 2020 respectively. Additionally, HCO_3^{-} represents the 20% of anions of 2018, 56% of 2019 and 53% of 2020. The groundwater of the alluvial show large quality variations, which are due to the

recharge conditions and the lithology of the formations within which it flows. They usually belong to the Ca-HCO_3 hydrochemical type. Possible sources of Na^+ result from ion exchange, in which clay minerals play the role of an exchanger.

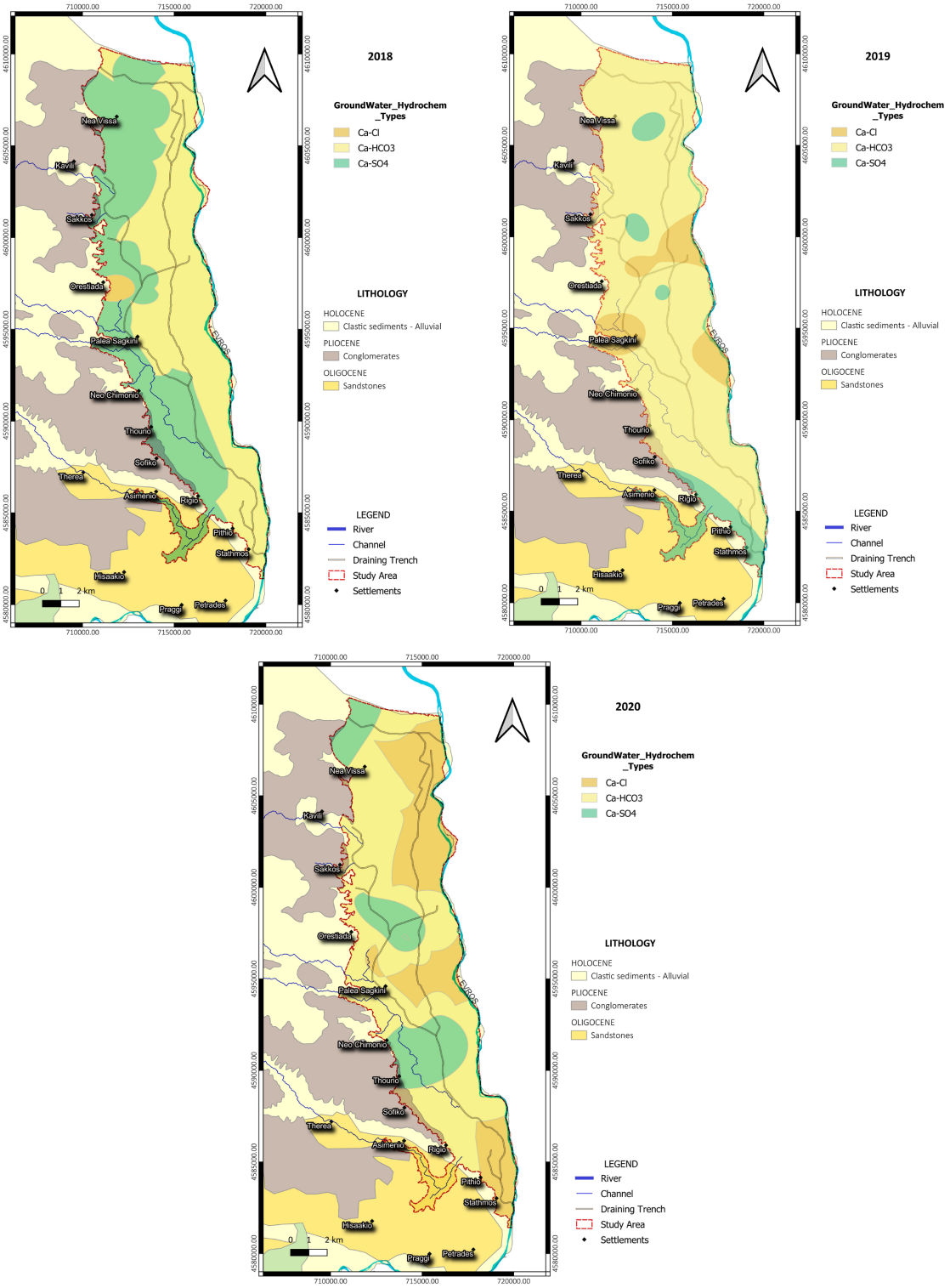

Figure 10. Spatial distribution of hydrochemical types of groundwater during sampling periods of 2018, 2019, 2020.

Figure 11. Spatial distribution of TDS for each campaign (2018, 2019, 2020).

As shown in Figure 11 and in Table 1, the TDS values of groundwater range from 126.75 mg/L to 1218.11 mg/L. It can be concluded that increasing trend of TDS value of groundwater occurs. The spatial distribution of TDS values as shown in Figure 11, are high in areas dominated by fine-grained materials (Figure 6). Due to the increased residence time of groundwater in the fine-grained materials and with the changes that occur in the rest of the aquifer resulting in a change in the hydrochemical state, ion exchange and mineral dissolution processes develop resulting in an increase in the TDS value. This is mainly due to the fact that the recharge of the aquifer system comes directly from surface water and precipitation is reduced. However, the groundwater is mainly freshwater with TDS < 1 g/L with exceedances in parts of the study area.

The Piper diagram (Piper, 1944) is an important tool for understanding hydrochemical characteristics, hydrochemical types, and hydrochemical evolution in groundwater. The type of groundwater chemistry is relatively complex in the study area. The hydrochemical evolution of groundwater moves from magnesium-carbonate type and calcium-bicarbonate to mixed sodium-carbonate and sodium-chloride types (Figure 12). In the temporal evolution of the groundwater flow and the interaction with the rock, an increase in the concentrations of Mg^{2+} and Na^{+} cations is observed, which can be interpreted as water discharge from neighboring aquifers or from anthropogenic activities, taking into account the standard deviation values and the results of the independent sample T-test. Among anions, the concentrations of HCO_3^- predominate in relation to SO_4^{2-} and Cl^- express continuous recharge of the underground aquifer system from surface water and precipitation.

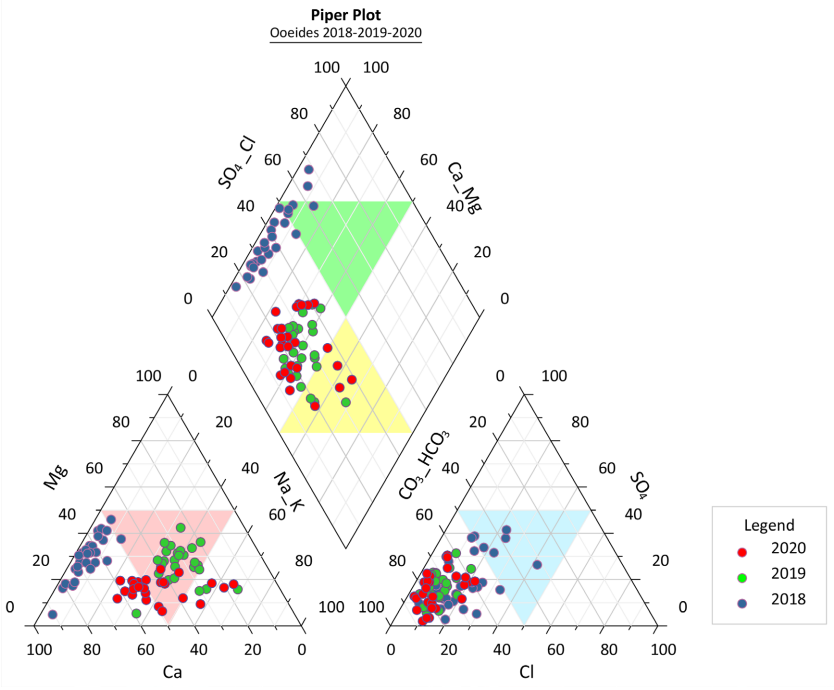

Figure 12. Piper plot.

Major ion relationships were designed to interpret the hydrochemical processes and control mechanism of local groundwater. The ion ratio relationship can further help to understand the process of water-rock interactions in this domain. Thus, according to the hydrochemistry data, ratio graphs of the major ion ratio were drawn (Figure 12).

In Figure 13(a), the Na^+/Cl^- molar ratio is approximately 1, indicating that halite dissolution is the main contributor to the groundwater Na^+ concentration. If this ratio is greater than 1, that means siliceous weathering or cation exchange is present, while if this ratio is less than 1, that represents an anthropogenic disturbance. The groundwater samples of 2019, 2020 were along and greater than 1 suggesting that halite dissolution, silicate weathering, and cation exchange are important sources of Na^+. All samples of 2018 located lower than the 1:1 trend line suggesting anthropogenic inputs.

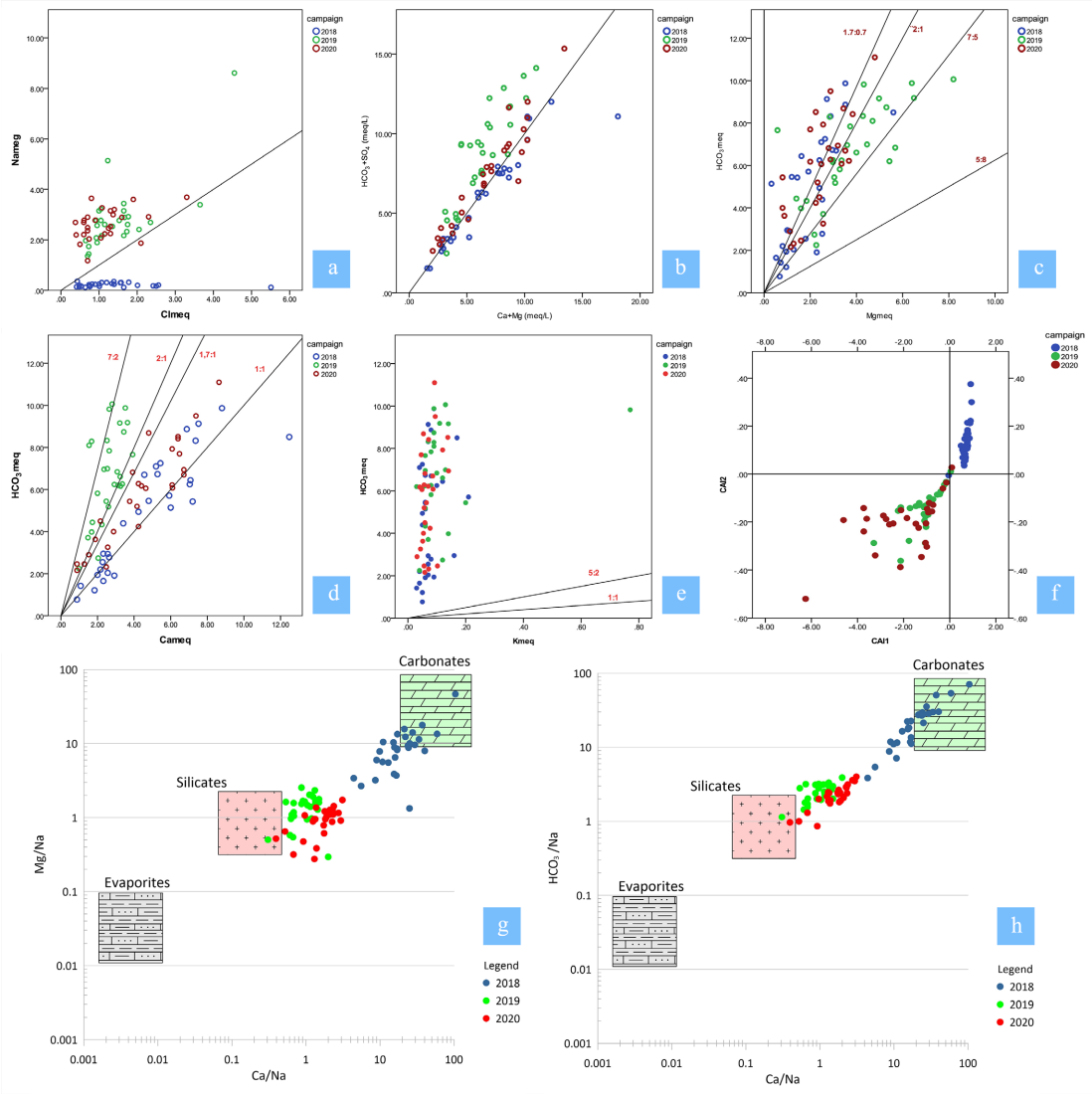

Figure 13. Diagrams: (a) Na vs Cl (meq/L); (b) $HCO_3 + SO_4$ vs Ca + Mg (meq/L); (c) HCO_3 vs Mg (meq/L); (d) HCO_3 vs Ca (meq/L); (e) HCO_3 vs K (meq/L); (f) chlorine-alkalinity index (CAI); (g) and (h) end diagrams.

In Figure 13(b), the plot of (Mg^{2+} + Ca^{2+}) versus (HCO_3^- + SO_4^{2-}) determines if dissolution of carbonate and sulfate minerals is the main reaction in groundwater samples. Most of the groundwater samples lie along the 1:1 trend line, implying the occurrence of soluble carbonates and gypsum minerals. In the samples located in the left area of the diagram, a reverse exchange of cations occurs in the groundwater, i.e. replacement of Na^+ and K^+ in the rock by Ca^{2+} and Mg^{2+} in the water. This procedure mainly concerns samples from the 2019 sampling period.

The Mg^{2+} and HCO_3^- relationship diagram (Figure 13(c)) has been used to reveal the sources of Mg^{2+} and HCO_3^- in groundwater. If Mg^{2+} and HCO_3^- come only from carbonate dissolution and weathering of amphibole, biotite and pyroxene, according to the chemical reactions, the ratio of HCO_3^-/Mg^{2+} will be: dolomite (line 2:1), amphibole (line 7:5), biotite (line 5:8) and pyroxene (line 1.7:0.7), respectively. The Mg^{2+} and HCO_3^- relationship is shown in Figure 13(c), where almost all samples lie along the 7:5 line and the 1.7:0.7 line, indicating a source of dissolution of dolomite, biotite and pyroxene.

Figure 13(d) presents graphs of Ca^{2+} and HCO_3^-. The ratios between Ca^{2+} and HCO_3^- as a result of mineral dissolution are 1:1 (limestone), 2:1 (dolomite and anorthite), 1.7:1 (pyroxene), 7:2 (amphibole). Figure 13(d) indicates that most water samples appear above the 1:1 line, indicating that HCO_3^- is greater than Ca^{2+} and that erosion of anorthite and dolomite is occurring. Water samples from 2019 and 2020 lie along the 1:1 trend line, suggesting that the main source of Ca^{2+} and HCO_3^- is calcite weathering. 2018 water samples are below the 1:1 line, indicating an excess of Ca^{2+}. 2019 water samples appear between the 2:1 and 7:2 lines suggesting that the main source of Ca^{2+} and HCO_3^- is dolomite weathering, anorthite and pyroxene.

If HCO_3^- and K^+ come mainly from the weathering of potassium feldspar (K-feldspar) and biotite, the HCO_3^-/K^+ ratio is 1:1 (K-feldspar) and 5:2 (biotite), respectively. As shown in Figure 13(e), all groundwater samples lie above the (1:1) line and the (5:2) line. This suggests that HCO_3^- is unnecessary in dissolution and that dissolution of potassium feldspar and biotite is rare in groundwater. HCO_3^- came mainly from the weathering of albite, plagioclast and carbonate minerals.

The chlorine-alkalinity index (CAI) is an important way to study cation exchange processes (Li et al., 2013; Huang et al., 2018). CAI-1 and CAI-2 are estimated through the following equations (ion units in meq/L):

$$\text{CAI-1}=\frac{Cl^- - \left(Na^+ + K^+\right)}{Cl^-} \tag{2}$$

$$\text{CAI-2}=\frac{Cl^- - \left(Na^+ + K^+\right)}{CO_3^{2-} + SO_4^{2-} + HCO_3^{2-} + NO_3^-} \tag{3}$$

If the chlorine-alkalinity index is less than 0, the normal cation exchange process dominates the hydrochemistry. Conversely, if the index is positive, a reverse cation exchange process takes place. Figure 13(f) showed that all 2019 and 2020

samples had negative chlorine-alkalinity index values, suggesting that Na^+ or K^+ in the aquifer has been replaced by Ca^{2+} or Mg^{2+} in the groundwater equation. The 2018 samples have positive index values, indicating a reverse cation exchange process. The reaction of decreasing Ca^{2+} and Mg^{2+} concentrations and increasing Na^+ concentration in groundwater is described by the following relationship (Hidalgo & Cruz-Sanjulián, 2001):

$$2Na^+(Clay)+\left(Ca^{2+}\ Mg^{2+}\right)\ \text{groundwater} \leftrightarrow \left(Ca^{2+}\ Mg^{2+}\right)\ (Clay)+2Na\ (\text{groundwater}) \quad (4)$$

Gaillardet et al. (1999) constructed an end-member diagram of the ion ratios between Ca^{2+}, Mg^{2+}, Na+ and HCO_3 (molar concentration) to determine the influence of the three main rock types (silicate, carbonate and evaporite) on water-rock interaction for the hydrochemical characteristics of an area. As shown in **Figure 13(g)** and **Figure 13(h)**, the groundwater sampling points mainly fell within a silicate and carbonate control zone, indicating that the chemical composition of the groundwater was affected by the dissolution of silicate and carbonate minerals.

The saturation index (SI) of a mineral can be estimated by the following equation: $SI = \log(IAP/K_{SP})$ (where IAP is the ion activity product for a mineral equilibrium reaction and K_{SP} is the solubility product of the mineral). PHREEQC software was used to calculate SI values of minerals in groundwater (Parkhurst & Appelo, 1999). SI results indicate the trend of water-mineral chemical equilibrium during water-rock interaction. If unsaturated ($SI < 0$), the mineral will be continuously eroded by groundwater. If it is supersaturated ($SI > 0$), the mineral will precipitate, and if SI is close to 0, the mineral phase will remain in equilibrium. According to the hydrochemistry data of the three periods, the saturation indices of specific minerals were calculated (**Table 4**).

Table 4. Saturation Index of Calcite, Dolomite, Gypsum, Halite, Hematite for each of sampling campaign.

	2018			2019			2020		
	mean	max	min	mean	max	min	mean	max	min
SI_Calcite	−1.81	1.69	−2.95	−2.00	−1.70	−2.52	−1.57	−0.23	−2.67
SI_Dolomite	−4.03	3.08	−6.05	−3.91	−3.30	−4.84	−3.43	−0.67	−5.14
SI_Gypsum	0.65	1.10	−0.49	0.55	0.86	−0.36	0.58	1.22	−0.35
SI_Halite	−5.52	−5.13	−6.09	−4.45	−3.41	−5.00	−4.57	−3.92	−5.04
SI Hematite	7.87	12.66	−10.00	6.20	11.23	−10.00	5.53	12.96	−10.00

The minerals contained in the aquifer sediments are the first priority of the possible mineral phases. In shallow aquifers, CO_2 and O_2 are also considered as possible phases. In addition, cation exchanges between Ca^{2+} and Na^+, Mg^{2+} and Na^+ are very important during groundwater chemical evolution processes (Shen & Zhu, 1993). Clay minerals were considered as adsorbents for cation exchange.

In all periods, the SI values of calcite, dolomite, gypsum and halite are negative. Therefore, these minerals are in a continuous process of dissolution, a fact that

expresses the continuous renewal of water in the groundwater system that results in ion exchange processes described by the diagram of chloralkaline indicators.

The SI values of the potential minerals calcite, dolomite, halite, were negatively correlated with TDS for 2018-2019 indicating that these minerals do not continue to dissolve along the flow path, while the SI of gypsum is positively correlated with TDS in 2018 indicating that the mineral continues to dissolve along the flow path and in 2019 is negatively correlated indicating that this mineral does not continue to dissolve along the flow path. In the period 2020, the SI values indicate hypocalcified (insufficient amount of calcium) minerals while they are positively correlated with TDS indicating that in this period unlike previous periods, minerals continue to dissolve along the flow. Common iron oxides and oxyhydroxides found in sediments are ferrihydrite, goethite, lepidocrocite, and hematite, which are among the most stable iron oxides. In all periods the SI values of hematite were mainly positive. Additionally, they were positive correlated with TDS for 2018-2019 but for 2020 were negatively correlated. Hematite precipitation often favors sulfate reduction. Hematite precipitation is noted in all sampling periods representing the oxidizing environment that dominates the underground aquifer system.

Increasing economic development, increasing human population and accelerating urbanization have led to increasingly negative impacts on the groundwater environment (Xiong et al., 2020). Anthropogenic inputs have thus become an important factor affecting the chemical composition of groundwater in many parts of the world (Eslami et al., 2019).

Groundwater in areas affected by intense human activities tend to contain increased amounts of Cl^-, NO_3^- and SO_4^{2-} (Fan et al., 2014; Xiao et al., 2016). Although Cl^- and SO_4^{2-} in groundwater may come from dissolution of evaporites (halite and gypsum, respectively), oxidation of sulphides or human industrial activities, NO_3^- in groundwater comes mainly from agricultural activities and domestic sewage. Contaminated groundwater generally exhibits higher Cl^-/Na^+ and NO_3^-/Na^+ molar ratios (Fan et al., 2014). Therefore, the nitrate content of a water body can reflect the degree of impact of human activities on the aquatic environment.

In general, water systems polluted by human activities are characterized by higher molar ratios of Cl^-/Na^+ vs NO_3^-/Na^+.

Figure 14 shows that in most of the groundwater sampling points, agricultural activities contribute the largest proportion to the concentration of SO_4^{2-} in the groundwater.

Also, the effect of NO_3^- from agricultural activities or municipal wastewater is small but continuous throughout the sampling periods. The anthropogenic inputs of nitrates, according to the relationship NO_3^-/Ca^{2+} vs SO_4^{2-}/Ca^{2+}, are related to the parts of the study area recharged by the Evros River at the eastern boundary of the study area (**Figure 15**). In addition, they are related to the location of the Wastewater Treatment Plant of the Municipality of Orestiada and to the settlements in the southern part of the area.

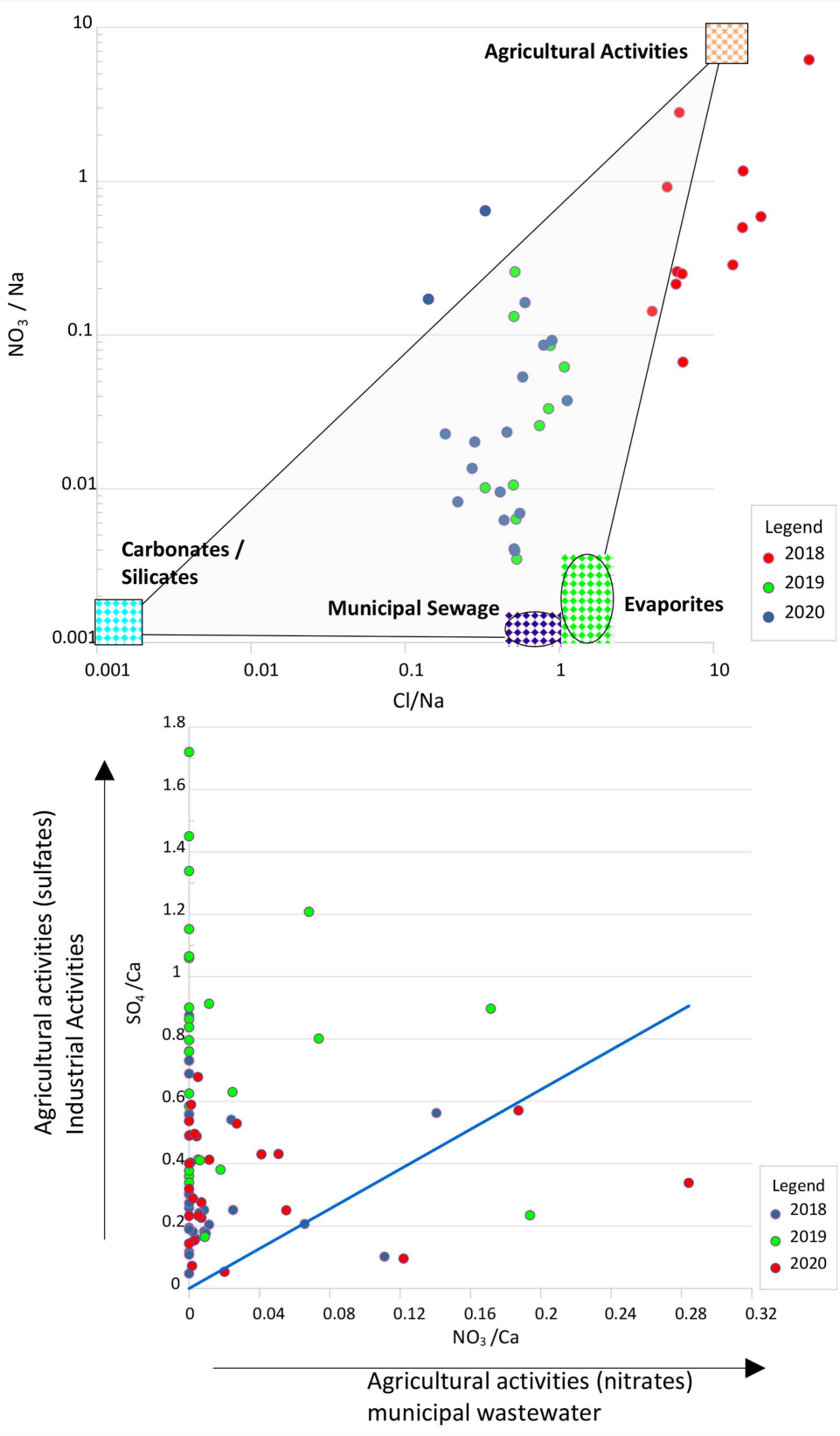

Figure 14. Molar ratios of the NO_3^-/Ca^{2+} vs SO_4^{2-}/Ca^{2+} (upper) and Cl^-/Na^+ vs NO_3^-/Na^+) (lower).

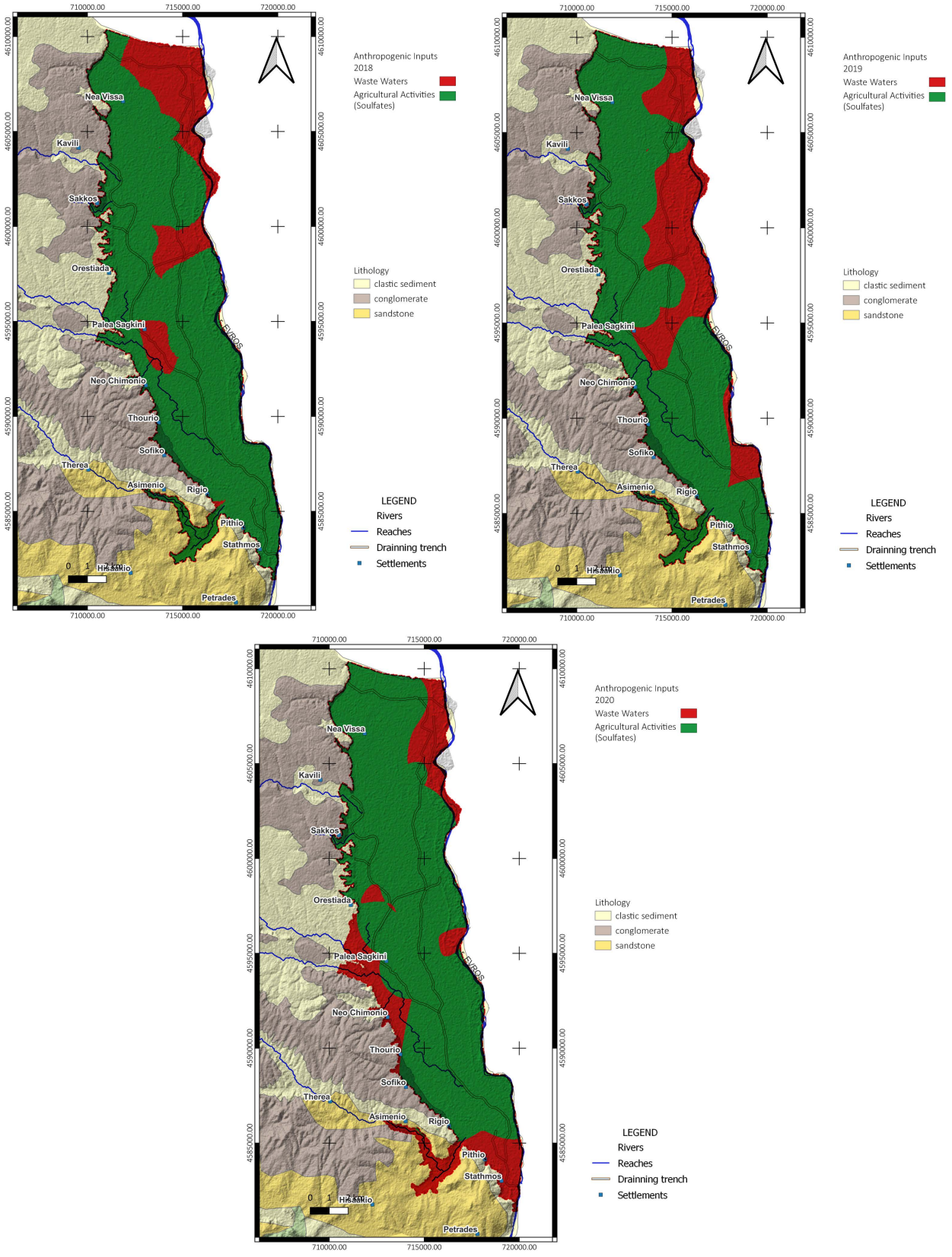

Figure 15. Anthropogenic inputs spatial analysis for 2018, 2019, 2020 (red colour represents municipality wastewaters influence. Green represents sulphates from agricultural activities).

5. Conclusion

This research work contributes to the evaluation of surface water and groundwater interactions, as well as water-rock interactions in the aquifer system of Ooeides, Orestiada Region, NE Greece, by assessing the quality of groundwater and the primary controls on groundwater chemistry in the study area. During sampling campaigns for the years 2018, 2019, and 2020, groundwater samples from the research region were analyzed using statistical analysis along with appropriate hydrochemical plots.

The hydrochemical evolution of groundwater, based on the Pipper diagram, moves from magnesium-carbonate type to mixed sodium-carbonate and sodium-chloride types. So, in 2018, groundwater samples, at a rate of 92%, are dominated by Ca-HCO_3, in 2019, at a rate of 71%, are dominated by Mg-HCO_3, and finally in 2020, the rate of 74% are Ca-HCO_3 type. In the first period, the groundwater type evolves from Ca-HCO_3 water to Ca-Mg-HCO_3 type. Precipitation infiltrates into the aquifer forming an acidic environment with the water-rock interaction leading to the dissolution of carbonates. In the following period, when there is a decrease in the annual amount of precipitation, the groundwater type evolves from Ca-Mg-HCO_3 to Na-HCO_3 type. In the third period, the evolution from Ca-Mg-HCO_3 to Na-HCO_3 type continues with a shift of the fresh groundwater.

In all periods the SI values of calcite, dolomite, gypsum and halite are negative. Therefore, these minerals are in a continuous process of dissolution, a fact that expresses the continuous renewal of water in the groundwater system that results in ion exchange processes described by the diagram of chloralkaline indicators. Additionally, hematite precipitation in all sampling periods represents the oxidizing environment that dominates the groundwater system.

Agricultural activities contribute the largest percentage to the SO_4^{2-} concentration in groundwater, while the effect of NO_3^- from agricultural activities or municipal wastewater is small but continuous throughout the sampling periods. The anthropogenic inputs of nitrates, according to the relationship NO_3^-/Ca^{2+} vs SO_4^{2-}/Ca^{2+}, are related to the parts of the study area that are recharged by the Evros River at the eastern boundary of the study area, as well as to the location of the Wastewater Treatment Plant of the Municipality of Orestiada and with the settlements in the southern part of the area.

The changes in the amount of precipitation affect the mechanism of groundwater hydrochemistry, although the participation of precipitation in the recharge of the aquifer is small. With the decrease of precipitation in the year 2019 by 262.47 mm, it is estimated that water from neighboring aquifers enters the studied aquifer taking into account the hydrochemical ratios diagrams.

The conjunctive use and the management of surface water and groundwater are a key factor for the development of the study area, taking into account the intense irrigation use due to the agricultural activities developed in the area. The investigation of the tectonic structures related to the groundwater flow and the recharge from neighboring and underlying aquifers, as well as the calculation of the

hydrological balance of the watersheds of the streams in the study area, are proposed to be the next stages of the research in the wider area.

Acknowledgements

The results of the paper are part of the research of the Doctoral Dissertation of Adam Adamidis, MSc geologist, Department of Civil Engineering, School of Engineering, Democritus University of Thrace, Greece.

Conflicts of Interest

The authors declare no conflicts of interest regarding the publication of this paper.

References

Adamidis, A., Despotakis, I., Kallioras, A., Angelidis, P., & Pliakas. F. K. (2022b). Conceptual Model of an Aquifer System in the Region of Orestiada, North Greece. In *Proceedings of the 12th International Hydrogeological Congress of Greece and Cyprus* (pp. 13-18). Cyprus Association of Geologists and Mining Engineers.

Adamidis, A., Kallioras, A., Angelidis, P., Gkiougkis, I., & Pliakas, F. K. (2022a). Assessment of Groundwater Quality in Ooeides Aquifer System, NE Greece. In *16th International Congress of the Geological Society of Greece* (pp. 474-475). Geological Society of Greece.

Adamidis, A., Kallioras, A., Gkiougkis, I., Angelidis, P., & Pliakas, F. K. (2023). Groundwater Resources Hydrochemical Evaluation in Ooeides Aquifer System, NE Greece. In *Proceedings of the 12th World Congress on Water Resources and Environment (EWRA 2023) "Managing Water-Energy-Land-Food under Climatic, Environmental and Social Instability"* (pp. 289-290). European Water Resources Association (EWRA).

Andronopoulos, B. (1977). Geological Study of Didymotichon-Pentalofos Area, Orestias Basin. *Geology & Geophysics Research, 17,* Article 59.

Ansari, M. A., Deodhar, A., & Kumar, U. S. (2019). Modeling of Geochemical Processes and Multivariate Statistical Analysis for Hydrochemical Assessment of Spring Water of the Outer Himalaya, India. *Environmental Earth Sciences, 78,* Article No. 665. https://doi.org/10.1007/s12665-019-8682-5

Aruga, R., Gastaldi, D., Negro, G., & Ostacoli, G. (1995). Pollution of a River Basin and Its Evolution with Time Studied by Multivariate Statistical Analysis. *Analytica Chimica Acta, 310,* 15-25. https://doi.org/10.1016/0003-2670(95)00101-5

Avtar, R., Kumar, P., Singh, C. K., & Mukherjee, S. (2011). A Comparative Study on Hydrogeochemistry of Ken and Betwa Rivers of Bundelkhand Using Statistical Approach. *Water Quality, Exposure and Health, 2,* 169-179. https://doi.org/10.1007/s12403-010-0035-2

Belkhiri, L., Mouni, L., & Tiri, A. (2012). Water-Rock Interaction and Geochemistry of Groundwater from the Ain Azel Aquifer, Algeria. *Environmental Geochemistry and Health, 34,* 1-13. https://doi.org/10.1007/s10653-011-9376-4

Choi, D. (1988). Formation of Jeju Island and the Characteristics of Groundwater. *Journal of Cheju Studies, 5,* 59-78.

Diamantis, I., & Pliakas, F. (2013). Geomorphological and Geological Environment of the Wider Area of River Ardas Basin—Land Use, Hydrogeological and Hydrological Research of River Ardas Drainage Basin, INTERREG Project: "Flood Warning System

Establishment in Arda River Basin for Minimizing the Risk in the Cross Border Area". *ARDA FORECAST*.

Dong, H., & Gao, Z. (2022). Theoretical Progress of Groundwater Chemical Evolution Based on Tóthian Theory: A Review. *Frontiers in Marine Science, 9,* Article 972426. https://doi.org/10.3389/fmars.2022.972426

Elango, L., & Kannan, R. (2007). Rock-Water Interaction and Its Control on Chemical Composition of Groundwater. In *Developments in Environmental Science* (pp. 229-243). Elsevier. https://doi.org/10.1016/s1474-8177(07)05011-5

Eslami, F., Yaghmaeian, K., Mohammadi, A., Salari, M., & Faraji, M. (2019). An Integrated Evaluation of Groundwater Quality Using Drinking Water Quality Indices and Hydro-Chemical Characteristics: A Case Study in Jiroft, Iran. *Environmental Earth Sciences, 78,* Article No. 314. https://doi.org/10.1007/s12665-019-8321-1

Fan, B., Zhao, Z., Tao, F., Liu, B., Tao, Z., Gao, S. et al. (2014). Characteristics of Carbonate, Evaporite and Silicate Weathering in Huanghe River Basin: A Comparison among the Upstream, Midstream and Downstream. *Journal of Asian Earth Sciences, 96,* 17-26. https://doi.org/10.1016/j.jseaes.2014.09.005

Gaillardet, J., Dupré, B., Louvat, P., & Allègre, C. J. (1999). Global Silicate Weathering and CO_2 Consumption Rates Deduced from the Chemistry of Large Rivers. *Chemical Geology, 159,* 3-30. https://doi.org/10.1016/s0009-2541(99)00031-5

Hem, J. D. (1985). *Study and Interpretation of the Chemical Characteristics of Natural Water. US Geological Survey Water Supply, Paper 2254*.

Hidalgo, M. C., & Cruz-Sanjulián, J. (2001). Groundwater Composition, Hydrochemical Evolution and Mass Transfer in a Regional Detrital Aquifer (Baza Basin, Southern Spain). *Applied Geochemistry, 16,* 745-758. https://doi.org/10.1016/s0883-2927(00)00078-0

Huang, X., Wang, G., Liang, X., Cui, L., Ma, L., & Xu, Q. (2018). Hydrochemical and Stable Isotope (δD and $\delta^{18}O$) Characteristics of Groundwater and Hydrogeochemical Processes in the Ningtiaota Coalfield, Northwest China. *Mine Water and the Environment, 37,* 119-136. https://doi.org/10.1007/s10230-017-0477-x

Koutles, T., Kassoli-Fournaraki, A., Filippidis, A., & Tsirambides, A. (1995). Geology and Geochemistry of the Eocene Zeolite-Bearing Volcaniclastic Sediments of Metaxades, Thrace, Greece. *Estudios Geológicos, 51,* 19-27. https://doi.org/10.3989/egeol.95511-2280

Ledesma-Ruiz, R., Pastén-Zapata, E., Parra, R., Harter, T., & Mahlknecht, J. (2015). Investigation of the Geochemical Evolution of Groundwater under Agricultural Land: A Case Study in Northeastern Mexico. *Journal of Hydrology, 521,* 410-423. https://doi.org/10.1016/j.jhydrol.2014.12.026

Li, P., Wu, J., & Qian, H. (2013). Assessment of Groundwater Quality for Irrigation Purposes and Identification of Hydrogeochemical Evolution Mechanisms in Pengyang County, China. *Environmental Earth Sciences, 69,* 2211-2225. https://doi.org/10.1007/s12665-012-2049-5

Liu, C., Lin, K., & Kuo, Y. (2003). Application of Factor Analysis in the Assessment of Groundwater Quality in a Blackfoot Disease Area in Taiwan Region. *Science of the Total Environment, 313,* 77-89. https://doi.org/10.1016/s0048-9697(02)00683-6

Liu, F., Zou, J., Liu, J., Zhang, J., & Zhen, P. (2022). Factors Controlling Groundwater Chemical Evolution with the Impact of Reduced Exploitation. *Catena, 214,* Article 106261. https://doi.org/10.1016/j.catena.2022.106261

Malenda, M. G. (2019). *Analysis of Anorthite Dissolution at the Microscopic Scale*. Master

Thesis, Colorado School of Mines.

Mu, X., Brower, J., Siegel, D. I., Fiorentino II, A. J., An, S., Cai, Y. et al. (2015). Using Integrated Multivariate Statistics to Assess the Hydrochemistry of Surface Water Quality, Lake Taihu Basin, China. *Journal of Limnology, 74*, 234-247. https://doi.org/10.4081/jlimnol.2014.906

Papadopoulos, K., & Romaidis, I. (2002). *Hydrogeological Research at the Wider Region of Ardas River Basin. Institute of Geology and Mineral Exploration (IGME), Regional Unit of Eastern Macedonia—Thrace (R.U.E.M.T. 2nd Community Support Framework (CSF)) (in Greek).*

Parkhurst, D. L., & Appelo, C. A. J. (1999). *User's Guide to PHREEQC (Version 2) a Computer Program for Speciation, Batch-Reaction, One-Dimensional Transport, and Inverse Geochemical Calculations: U.S Geological Survey Water-Resources Investigations Report, 99-4259*. https://pubs.er.usgs.gov/publication/wri994259

Piper, A. M. (1944). A Graphic Procedure in the Geochemical Interpretation of Water Analyses. *American Geophysical Union, Transactions, 25,* 914-923. https://doi.org/10.1029/TR025i006p00914.

Razi, M. H., Wilopo, W., & Putra, D. P. E. (2024). Hydrogeochemical Evolution and Water-Rock Interaction Processes in the Multilayer Volcanic Aquifer of Yogyakarta-Sleman Groundwater Basin, Indonesia. *Environmental Earth Sciences, 83,* Article No. 164. https://doi.org/10.1007/s12665-024-11477-6

Ribinu, S. K., Prakash, P., Khan, A. F., Bhaskar, N. P., & Arunkumar, K. S. (2023). Hydrogeochemical Characteristics of Groundwater in Thoothapuzha River Basin, Kerala, South India. *Total Environment Research Themes, 5,* Article 100021. https://doi.org/10.1016/j.totert.2022.100021

Salyapongse, S., Kositanont, S., Jirajesda, J., & Fontaine, H. (2022). *Constraints on Playa Lake Deposition of the Maha Sarakham Formation with Its Association of Sodium Carbonate and Sodium Sulfate—Bearing Minerals in Thailand*.

Shen, Z. L., & Zhu, W. H. (1993). *Hydrogeochemical Basis*. Geological Publishing House.

Singh, K. P., Malik, A., Mohan, D., & Sinha, S. (2004). Multivariate Statistical Techniques for the Evaluation of Spatial and Temporal Variations in Water Quality of Gomti River (India)—A Case Study. *Water Research, 38,* 3980-3992. https://doi.org/10.1016/j.watres.2004.06.011

Singh, S., Ghosh, N. C., Gurjar, S., Krishan, G., Kumar, S., & Berwal, P. (2018). Index-Based Assessment of Suitability of Water Quality for Irrigation Purpose under Indian Conditions. *Environmental Monitoring and Assessment, 190,* Article No. 29. https://doi.org/10.1007/s10661-017-6407-3

Sunkari, E. D., Seidu, J., & Ewusi, A. (2022). Hydrogeochemical Evolution and Assessment of Groundwater Quality in the Togo and Dahomeyan Aquifers, Greater Accra Region, Ghana. *Environmental Research, 208,* Article 112679. https://doi.org/10.1016/j.envres.2022.112679

Tesfamichael, T. A. (2011). *Water-Rock Interaction and Geochemistry of Groundwater in Axum Area (Northern Ethiopia)*. Doctoral Dissertation, Graz University of Technology Institute of Applied Geosciences.

Tsirambides, A., Filippidis, A., & Kassoli-Fournaraki, A. (1993). Zeolitic Alteration of Eocene Volcaniclastic Sediments at Metaxades, Thrace, Greece. *Applied Clay Science, 7,* 509-526. https://doi.org/10.1016/0169-1317(93)90019-w

Xiao, J., Zhang, F., & Jin, Z. (2016). Spatial Characteristics and Controlling Factors of Chemical Weathering of Loess in the Dry Season in the Middle Loess Plateau, China.

Hydrological Processes, 30, 4855-4869. https://doi.org/10.1002/hyp.10959

Xiong, G., An, Q., Fu, T., Chen, G., & Xu, X. (2020). Evolution Analysis and Environmental Management of Intruded Aquifers of the Dagu River Basin of China. *Science of the Total Environment, 719,* Article 137260. https://doi.org/10.1016/j.scitotenv.2020.137260

Zhang, X., Qian, H., Wu, H., Chen, J., & Qiao, L. (2016). Multivariate Analysis of Confined Groundwater Hydrochemistry of a Long-Exploited Sedimentary Basin in Northwest China. *Journal of Chemistry, 2016,* 1-15. https://doi.org/10.1155/2016/3812125